Hybrid superconducting-ferroelectric quantum memristor

Maria A. Badarne [1,2] Emanuele G. Dalla Torre [3] and Yachin Ivry [1,2,4,5]

[1]Department of Materials Science and Engineering, Technion Israel Institute of Technology, Haifa 3200003, Israel
[2]Solid State Institute, Technion Israel Institute of Technology, Haifa 3200003, Israel
[3]Department of Physics, Bar-Ilan University, Ramat Gan 5290002, Israel
[4]Department of Materials Science and Engineering, University of California, Berkeley, California 94720, USA
[5]Grand Technion Energy Program, Technion Israel Institute of Technology, Haifa 3200003, Israel

(Received 19 August 2024; revised 25 April 2025; accepted 3 November 2025; published 1 December 2025)

The nontrivial integration of qubits with classical computing systems and the lack of quantum-memory devices remain a key obstacle in the development of quantum technologies. Here, we present a theoretical platform for hybrid quantum devices with memory characteristics. In these current-driven hybrid memristors, a ferroelectric layer serves as the tunneling barrier in a superconducting Josephson junction; thus, the potential barrier is history-dependent. A memory-integrated phase qubit and a Lagrangian description of the superconducting circuit are also presented, paving the way to highly functional, self-modulated Josephson-junction technologies.

DOI: 10.1103/4746-w9cm

I. INTRODUCTION

The rapidly growing demand for Artificial Intelligence and neuromorphic data processing is driving the development of suitable hardware. A combination of memory and computing capabilities in a single device, a memristor, addresses this need, while it is also promising for reducing power consumption. Ferroelectric tunnel junctions (FTJs) [Figs. 1(a) and 1(b)] enable such memristors [1–4] by utilizing the nonvolatile polarization retention of ferroelectrics. In FTJs, electric current flows through a thin ferroelectric layer sandwiched between two electrodes. The tunneling barrier is asymmetric due to the ferroelectric intrinsic polarization, and the current flow is thus history-dependent. Specifically, current flows easily in one direction and encounters a large potential barrier that impedes the flow in the other direction, such that the current flow defines the bit's binary state. However, if the current and resulting voltage are sufficiently high to induce polarization reversal, the potential barrier reverses, as does the resistance that the current encounters.

Given the growing interest in quantum computing, it is compelling to incorporate memristive characteristics in the quantum arena. Superconducting Josephson junctions (JJs) are a key platform for quantum computing. Intuitively, replacing the FTJ switching electrodes with superconductors establishes a quantum memristor [Figs. 1(c) and 1(d)]. The ferroelectric thin film functions as tunable barrier in such a device, utilizing the nonvolatile polarization that is reversible with an external bias via a hysteresis loop [Fig. 1(e)]. Moreover, such devices would benefit from a significant reduction in power consumption due to the absence of resistance in superconductors. A closely related approach to realizing memory and computing functionalities is found in superconductor-ferromagnet-superconductor Josephson junctions [5–7]. The discovery of a Josephson diode effect has indeed garnered much attention recently [8–13], because the JJ quantum state is controllable with the driving current without using magnetic fields, which impose a large device footprint and additional power consumption. Yet, the lack of resistance and thus of a built-in voltage in superconductors imposes symmetric tunneling probability and thus current flow across a JJ, regardless of the polarization orientation, preventing a superconducting-ferroelectric-superconducting quantum memristor.

Here, we propose that symmetry breaking between the two polarization directions becomes possible when one electrode is thin enough for the ferroelectric state to significantly affect the superconducting charge-carrier density [Fig. 1(f)], allowing us to control the JJ quantum properties. The effect was analyzed with the Lagrangian formalism with single-valued mapping to the resistively and capacitively shunted junction (RCSJ) [14] model for JJs [Fig. 1(g)].

Recent observations indicate that the charge modulation becomes significant [15] when the superconducting thickness is comparable to the Thomas-Fermi screening length [16–18] [Fig. 1(f)]. Practically, JJs and qubits with 10 nm and even two-dimensional superconducting films have been demonstrated experimentally [19,20]. Consequently, the up and down polarization states of the ferroelectric barrier modulate the superconducting critical current of the thin electrode [Fig. 1(f)], which serves as the bottleneck for the JJ critical current. To demonstrate the memristive effect of this hybrid device, we show that the anharmonic energy profile of the qubit is controlled by the current-driven, nonvolatile polarization state of the barrier.

The characteristics of the superconducting-ferroelectric-superconducting device can be extracted from its Hamiltonian, which comprises three parts: the superconductive JJ, the ferroelectric barrier, and the

Published by the American Physical Society under the terms of the Creative Commons Attribution 4.0 International license. Further distribution of this work must maintain attribution to the author(s) and the published article's title, journal citation, and DOI.

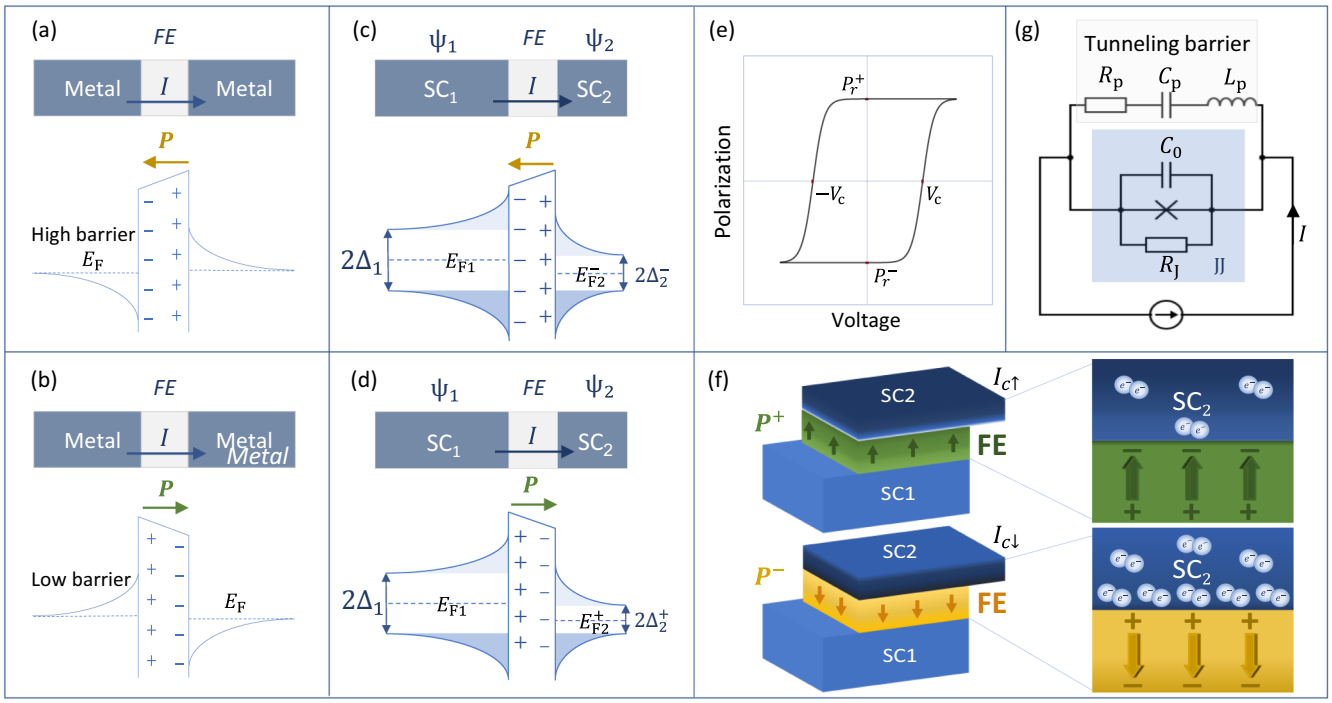


FIG. 1. Schematic description of normal and quantum ferroelectric tunnel junctions. (a), (b) A ferroelectric tunnel junction sandwiched between normal metallic electrodes, with the energy band structure demonstrating the dependence of the tunneling barrier on the polarization state [1]. (c), (d) A superconducting-ferroelectric-superconducting (SFES) tunnel junction with asymmetric electrodes and the corresponding energy band structure, illustrating asymmetric current flow that depends on the ferroelectric polarization state. (e) Typical ferroelectric polarization-voltage hysteresis loop. (f) Side view of the asymmetric SFES junction, with up (top) and down (bottom) polarization states and a closer look at the polarization-dependent current flow in the asymmetric SFES, arising from charge-induced modulations of the superconducting energy gap within the Thomas-Fermi screening depth. (g) Equivalent electrical circuit of the current-driven SFES junction, following the resistively and capacitively shunted junction (RCSJ) model [14].

superconducting-ferroelectric (SC-FE) coupling. The superconductive JJ Hamiltonian [21]

$$H_{JJ} = E_c + U_\varphi \tag{1a}$$

describes the capacitance energy $E_c = \frac{Q^2}{2C_J}$ and the JJ tilted washboard potential energy $U_\varphi = -\frac{\hbar I_c}{2e}\cos(\varphi) - \frac{\hbar I_{bias}}{2e}\varphi$. Here, $Q = ne$ is the total charge that is stored in the junction, e is the electron charge, n is the charge carrier number, C_J is the junction's capacitance, I_c is the critical current that determines the potential depth, $\varphi = \theta_2 - \theta_1$ is the phase difference across the tunnel junction, and I_{bias} is the bias current that sets the potential tilt.

The energy of the ferroelectric tunneling barrier is described by the simplified [22] double-well Devonshire adaptation of the Ginzburg Landau [23,24] free energy and is given by the volume integral:

$$H_{FE} = \int D(q+q_0)^2(q-q_0)^2 + \rho\frac{p^2}{2m_{eff}}dv. \tag{1b}$$

Here, D is the Landau-Devonshire coefficient and q is the polarization charge (the main coordinate) with an equilibrium value q_0 [25], ρ is the charge density, p is the canonically conjugate of q (its momentum), and m_{eff} is the polarization inertia effective mass under an electric field [26–28].

Previous works showed that in a ferroelectric-superconductive bilayer, superconductive properties, such as I_c (the critical current) and R_n (the normal resistance), vary between positive and negative ferroelectric polarization [2,15,18]. This change is attributed to the Thomas-Fermi screening that modulates the superconducting pseudo-wavefunction amplitude, i.e., the energy gap that in turn governs the superconducting charge carrier density. These effects are modeled by $I_c = I_{c0}(1+\alpha q)$, where I_{c0} is the critical current in the absence of a ferroelectric barrier and α represents the ferroelectric-superconductive coupling. Thus, the total SFES Hamiltonian is given by

$$H_{SFES} = \frac{1}{2}\frac{(en)^2}{2C_J} - \frac{\hbar I_{c0}}{2e}(1+\alpha q)\cos(\varphi) - \frac{\hbar I_b}{2e}\varphi + \int D(q+q_0)^2(q-q_0)^2 + \rho\frac{p^2}{2m_{eff}}dv\,. \tag{1c}$$

Using the Lagrangian formalism, the canonical Euler-Lagrange equations were derived:

$$\frac{\partial p}{\partial t} = m_{eff}\frac{\partial^2 q}{\partial t^2} = V_J - \frac{\hbar I_{c0}}{2e}\alpha\cos(\varphi) - Aq + Bq^3, \tag{2a}$$

$$\frac{\partial q}{\partial t} = \frac{p}{m_{eff}}, \tag{2b}$$

$$\frac{\partial n}{\partial t} = \frac{I_b}{2e} - \frac{I_{c0}}{2e}(1+\alpha q)\sin(\varphi) - \frac{V_J}{R_J(1+\eta q)}, \tag{2c}$$

$$\frac{\partial \varphi}{\partial t} = \frac{e^2}{2C_J\hbar}n = \frac{eV_J}{2\hbar}. \tag{2d}$$

Here, the derivatives are with respect to time. A dissipative term was introduced to Eq. (2c), describing energy relaxation in the JJ (normal resistance), and the ferroelectric dissipation was neglected. Equation (1c) assumes energy conservation. Thus, the additional voltage that develops across the JJ in the normal state (V_J) should be added in the derived equations of motion [Eqs. (2a)–(2d)]. To complete the description of the junction, we considered the energy relaxation as a linear resistor R_J that depends on the polarization charge of the junction: $R_J \to R_J(1+\eta q)$, where η is a resistance-polarization coupling parameter [15].

The main source of dissipation originates from quasiparticles' decay and can be effectively described as a shunt resistor [29], obeying the quantum fluctuation-dissipation theorem. For such a system, introducing quantum fluctuations is straightforward; see, for example, the Caldeira and Leggett model [30] for the case of an Ohmic bath.

Note that Eq. (2c) describes a combination of charge flow with a displacive current. Due to the ferroelectric polarization, the bound charge adds to the JJ native capacitance. Therefore, it is convenient to introduce a charge-modifying factor α' and consider [Eq. (2d)] the effective total charge that corresponds to the total voltage (V_J) applied across the junction: $\frac{ne\alpha'}{2C_J} = \frac{Q_{\text{eff}}}{C_J}$. Where α' is directly proportional to the dielectric constant of the ferroelectric barrier and Q_{eff} is the total effective charge on the junction considering the polarization screening effect. The term $-\frac{\hbar I_{c0}}{2e}\alpha\cos(\varphi)$ in Eq. (2a) represents the change in the double-well potential as a result of the SC-FE coupling, calculated to be small and negligible.

An alternative intuitive derivation of Eq. (2) relies on the equivalent circuit of the SFES [Fig. 1(c)], and applying Kirchhoff's circuit laws, a similar approach was demonstrated recently to show a resonance effect in a JJ with a single-well (paraelectric) barrier. [26] The resulting set of equations is then mapped directly to Eqs. (2a)–(2d) when the ferroelectric-superconductive coupling is added:

$$L\frac{\partial p}{\partial t} = V - q_0\alpha\cos(\varphi) - Aq + Bq^3, \tag{3a}$$

$$\frac{\partial q}{\partial t} = p, \tag{3b}$$

$$\frac{\partial V}{\partial t} = I - (1+\alpha q)\sin(\varphi) - \beta(q)V - \frac{\partial q}{\partial t}, \tag{3c}$$

$$\frac{\partial \varphi}{\partial t} = V. \tag{3d}$$

Here, $L = \omega_p^2 C_0 m_{\text{eff}}$ is normalized inductance of the system, C_0 is the JJ capacitance, $V = \frac{V_J}{V_0}$ is the normalized voltage (V_0 is the voltage for a JJ with a nonferroelectric barrier), $I = \frac{I_{\text{bias}}}{I_{c_0}}$ is the normalized current, $A = Bq_0^2$ and B are the Landau-Devonshire coefficients, and $\beta = \frac{1}{\beta_{\text{SM}}} = \frac{1}{C_0\omega_p R_J}$ is the inverse of the Stewart-McCumber [31,32] parameter $\beta_{\text{SM}} = C_0\omega_p R_J$. The ferroelectric-superconducting coupling is introduced here by the polarization-dependent resistance and critical current as was demonstrated both theoretically [33,34] and experimentally [15,35–38]. This twofold dependence is not surprising, given that $I_c R_n \propto \Delta$ [39]. In the normalized set of Eqs. (3), $\omega_p = \sqrt{\frac{2eI_c}{\hbar C_0}} = \sqrt{\frac{2\pi}{\Phi_0}\frac{I_c}{C_0}}$ is the plasma frequency of the JJ and $q_1 = \frac{P}{q_0} = \frac{P\omega_p}{I_c}$ is the normalized polarization charge, where V and I are the normalized voltage and current, respectively. In the current work, I_c (and hence Δ) of one superconducting electrode of the junction is modulated dramatically, while the other remains unchanged due to the difference in thickness between the electrodes.

The duality and one-to-one correspondence (see Table S1 in the Supplemental Material for details [40]) between the fundamental Hamilton-Jacobi derivation [Eqs. (2a)–(2d)] and the equivalent-circuit Kirchhoff's equation framework [Eqs. (3a)–(3d)] help simplify modeling of complex JJ circuits and devices and extend beyond the present ferroelectric-integrated devices and can be implemented beyond the scope of the SFES device that is discussed here.

To simulate the experimental properties of the SFES junction, Eqs. (2) and (3) were numerically solved while slowly varying the driving current. The physical parameters (e.g., voltage and polarization) were then extracted after the system relaxed to a quasistatic state. Two simulation protocols were chosen to highlight the dependence of the device properties (voltage and polarization) on the driving parameter (current) history and hence demonstrate a memory effect. These include a complete hysteresis cycle and a positive-up-negative-down-up (PUNDU) current variation cycle [41].

II. RESULTS

Figure 2 shows the SFES current-modulated polarization and voltage, extracted from the normalized Eqs. (3a)–(3d). In this figure, we implemented the PUNDU hysteresis protocol, commonly used to describe the behavior of ferroelectric materials and represented by arrows in Fig. 2. According to this protocol the bias current increases from the initial bias point at the first segment P: $I = 0$ up to $I = 3$, which is then repeated in U, followed by N: from $I = 0$ to $I = -3$, and D: from 0 to $I = -3$, and the protocol ends with the last segment U: from $I = -3$ to $I = 3$. History-dependent hysteretic behavior was found, where the polarization switches at a certain path-dependent current value, I_{switch}. See Supplemental Material [40] for the analysis of a different current path demonstrating the same memristive effect. Bearing in mind the effect of polarization on the tunneling potential, Eqs. (3a)–(3d) indeed lead to asymmetric I-V behavior, as demonstrated in Fig. 2(b). Fig 2(b) shows that the junction exhibits typical JJ I-V curve, with one main exception: The superconducting device critical currents for positive and negative values with respect to the polarization orientation (I_c^+ and I_c^-, respectively) are not identical. The asymmetry in polarization-switching and critical current values originates from a change in the normal resistance between the two polarization states [2], which following Ohm's law imposes variation in current values for maintaining a similar switching voltage [Fig. 2(b)]. The weak polarization difference between branches D and U in Fig. 2(a) stems from the voltage hysteresis of the junction, common to underdamped Josephson junctions. Because the

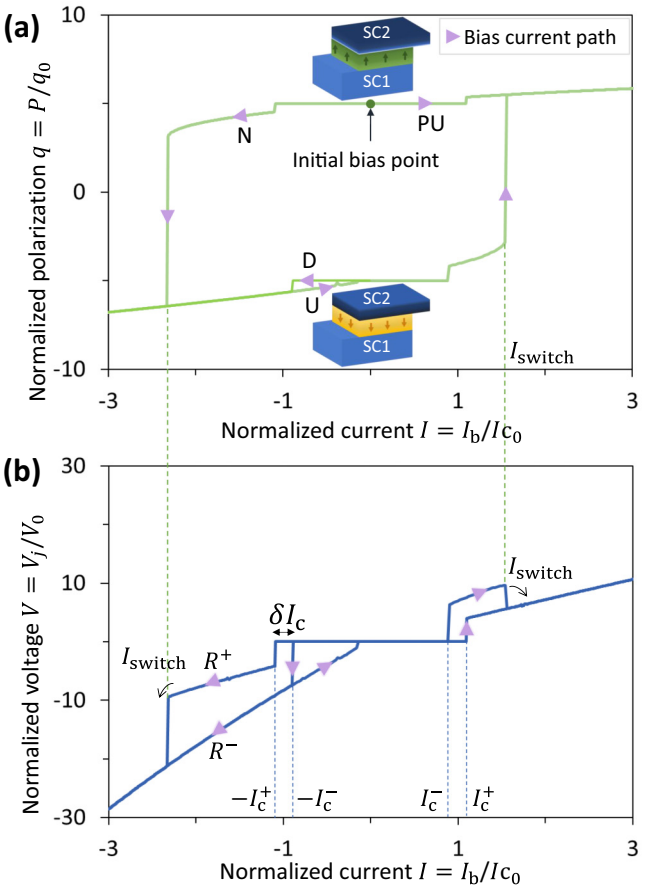


FIG. 2. Dynamics of the SFES Josephson junction—memory effect. (a) Current-driven hysteretic behavior of an SFES JJ, following Eqs. (3a)–(3d), demonstrating up (+) and down (−) polarization-switching current values (I_{switch}). (b) Calculated voltage for the same driving-current profile, illustrating dependence of the critical current (I_c^+ /I_c^-) and normal resistance (R^+/R^-) on the polarization orientation. Arrows designate the current trajectory, which is typical for a ferroelectric memory device. Horizontal dashed lines show symmetric polarization switching with respect to the voltage.

voltage difference between the two branches is small, the polarization is slightly off the equilibrium value P^- but is not switched.

Realization of an SFES device depends on the parameters of the chosen materials and the precise dimensions of the JJ and its barrier [15,19,20,26,42–47]. Here, a simple SFES junction was considered (see methods in the Supplemental Material [40]) to simulate the junction and get a general understanding of the dynamics.

Figure 2 presents a memristive behavior of a quantum device (JJ) that comprises a memory effect and a current-dependent resistance. The memory effect of the superconductive properties is demonstrated, however, mainly by means of polarization-dependent classical observables, such as critical current and normal resistance, which can be seen as $I_c^{+/-}$ and $R^{+/-}$ in Fig. 2(b). Yet, the polarization switching requires voltage, so that the polarization switching current is larger than the superconducting critical current. This also means that the polarization state affects the quantum state of the device for currents smaller than $|I_c^{+/-}|$. These properties help introduce memristive behavior to semiclassical systems, such as rapid single-flux quantum. Yet, there is a high motivation for illustrating memristive behavior also for superconductive quantum properties for introducing a device whose quantum properties depend on its history. Figure 2 supports the idea of utilizing the SFES device for introducing a memory effect in qubits. The quantum behavior of a superconductive device is described by the pseudo-wavefunction $\psi = \Delta e^{i\theta}$ with an amplitude Δ and phase θ. Here, we chose to exemplify the effect on a phase qubit. Expanding the benefit of memory effects to additional quantum technologies is straightforward, e.g., by introducing a capacitor in series for obtaining a charge qubit [21].

Phase qubits are common and relatively simple qubits that are described by a tilted washboard potential, $U_\varphi = -\frac{\hbar I_c}{2e}\cos(\varphi) - \frac{\hbar I_{bias}}{2e}\varphi$ [Eq. (1a)]. Figure 3(a) demonstrates the dependence of U_φ on I_{bias} and I_c for a regular qubit ($P = 0$) as well as an SFES qubit with up (P^+) and down (P^-) polarization states; the potential energy was calculated using the critical current I_c for a nonferroelectric barrier, and I_c^+ and I_c^- for the up and down polarization as calculated based on previous experiment [15]. A phase qubit operates at a regime where the phase is trapped in an energy well that serves as an anharmonic potential within the sinusoidal potential due to a balance between the potential tilt and depth. Typically, this occurs at Fig. 3(b), or close to Fig. 3(c), a zero-bias current. Increasing the current induces a tilt in the phase profile and effectively decreases potential depth (as well as the potential barrier between adjacent local energy minima), so eventually, above I_c, the device cannot serve anymore as a qubit [Fig. 3(d)].

Figure 3(c) shows the phase evolution for different current values for both positive (green) and negative (yellow) polarization states of the SFES. The different behaviors of the qubit between the two polarization states emphasize the memory effect of the quantum device at its quantum state.

Figure 3 helps illustrate the memristive effect on the devices quantum state. When no current (or a small current) is applied [Figs. 3(b) and 3(c)], a constant-phase equilibrium state maintains the superconducting state with the driving force $V \propto \frac{\partial\varphi}{\partial t}$ equal to zero. The potential depth determines the plasma frequency and hence the gap between the two lowest-energy states, $E_{01} = \hbar\omega$, of the anharmonic potential. However, the depth, which is set by I_c, is determined by the polarization orientation [Fig. 2(b)]. Thus, the energy gap of this two-level system is also polarization dependent. This energy gap, $\hbar\omega_{+/-}$, defines the qubit state as well as the readout frequency, so that the difference between $\hbar\omega_+$ and $\hbar\omega_-$ [Fig. 3(b)] demonstrates that the qubit state is controlled with polarization. The polarization itself is set by the history of the current path [Fig. 2(a)], so that memory is introduced to the qubit by its own driving current. Finally, the ability to increase the potential depth with polarization is promising for overcoming phase slips [48] and hence stabilizing the quantum state for longer operational times.

The ferroelectric degrees of freedom enter into the equations of motion as energy-preserving terms and their only effect is to modify the effective potential of the phase degrees of freedom, as schematically shown in Fig. 3. Since the main

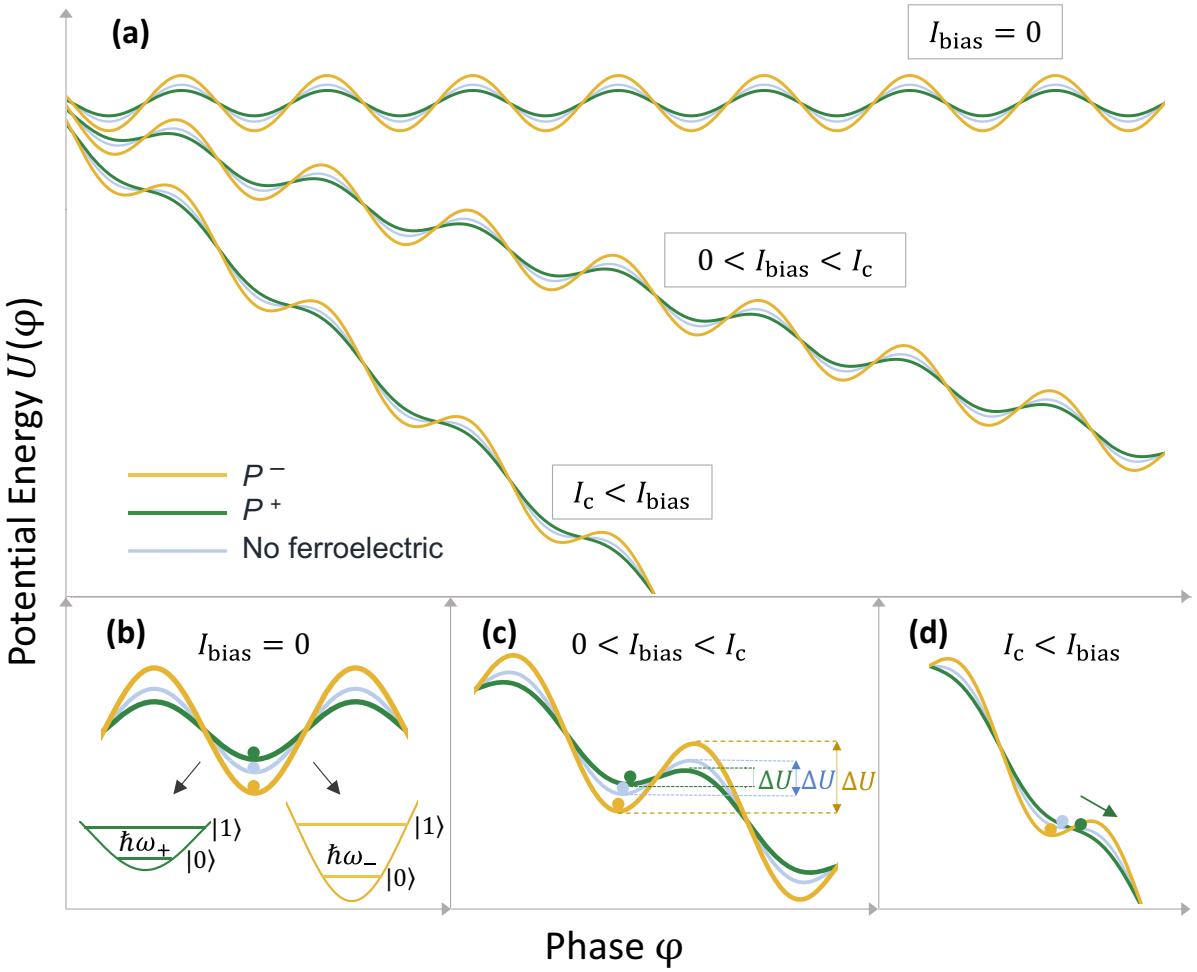


FIG. 3. Phase-qubit SFES memristor. (a) Potential-energy profile (U_φ, calculated) of a Josephson junction with a nonferroelectric barrier (light blue) and SFES with up (green) and down (yellow) polarization phase qubits, for different bias currents. (b) A closer look at $U(\phi)$ under zero bias current shows that the energy gap of the two-level system is tunable with polarization ($\hbar\omega_{+/-}$). (c) Increasing the bias current and remaining below I_c maintains the memristive behavior, while (d) increasing I_b further, above the critical value, removes the device from its quantum state and the phase-qubit framework.

goal of the present work is to describe in a quantitative manner the functionality of a device that combines the capabilities of superconducting tunnel junctions and ferroelectric materials, we focus our description on the salient aspects that highlight the uniqueness of our device, rather than dwelling on well-known effects. For completeness, the dissipation in the insulator, the ferroelectric barrier, is described by the loss tangent $\tan\delta = \mathrm{Im}\{\epsilon\}/\mathrm{Re}\{\epsilon\}$, where ϵ is the dielectric constant of the ferroelectric. Recent work on ultralow-loss ferroelectrics has shown dissipative effects in ferroelectric thin films ($\tan\delta < 0.002$) demonstrating a damping coefficient compatible with those required for state-of-the-art qubit [46].

It should be noted that the above JJ (Fig. 2) is underdamped. Although such devices garner interest for superconductive logic circuits [43], an overdamped junction can be realized simply by introducing shunt resistance and impedance that prevent the junction from latching [49].

We would like to draw attention to a recent preliminary study of SFES that shows another type of ferroelectric-superconductive coupling [26]. Here, an SFES JJ was used to demonstrate a joint ferroelectric-superconducting resonance mode. The authors used the ferroelectric high dielectric constant for this application; however, the material was considered paraelectric, with no remnant polarization. That is, following Eq. (3a), the ferroelectric had a single-well and not a double-well potential, the cubic coefficient of q at the double well was set to zero, and no remnant polarization or polarization switching exists in the system. The existence of such resonance modes appears also in our calculations, which is given in the form of small kinks in the I-V curve (at around $I = 0.8$; see Fig. S1 in the Supplemental Material [40]).

To conclude, the SFES junction operates as a hybrid classical bit in the normal state where it operates as a memristor and as a quantum bit in the superconducting state where it operates as a phase qubit, in which the energy gap between the two lowest states $\hbar\omega_{+/-}$ is tunable by the ferroelectric barrier polarization switching.

ACKNOWLEDGMENTS

This research was carried out within the framework of the UConn—Technion Energy Collaboration Initiative,

supported by the Satell Family Foundation, the Maurice G. Gamze Endowed Fund (at the American Technion Society), Larry Pitt and Phyllis Meloff, The Eileen and Jerry Lieberman UConn/Israel Global Partnership Fund, Cohen Family UConn—Israel Start Up Fund, and the Grand Technion Energy Program (GTEP). M.A.B. thanks the Neubauer Family Foundation for their generous support of her doctoral research. The authors thank Prof. Michael Stern for fruitful discussions. Y.I. thanks Prof. Lane W. Martin for kind sabbatical hospitality when working on the project.

The authors declare that there is no conflict of interest.

All authors contributed to the work and paper writing. M.A.B. wrote the derivations and ran the simulations. Y.I. initiated and supervised the project. E.G.D.T. supervised the project.

[1] V. Garcia and M. Bibes, Ferroelectric tunnel junctions for information storage and processing, Nat. Commun. **5**, 4289 (2014).

[2] S. C. Chang, A. Naeemi, D. E. Nikonov, and A. Gruverman, Theoretical approach to electroresistance in ferroelectric tunnel junctions, Phys. Rev. Appl. **7**, 024005 (2017).

[3] C. Ma *et al.*, Sub-nanosecond memristor based on ferroelectric tunnel junction, Nat. Commun. **11**, 1439 (2020).

[4] Z. Wen and D. Wu, Ferroelectric tunnel junctions: Modulations on the potential barrier, Adv. Mater. **32**, 1904123 (2020).

[5] A. Vettoliere *et al.*, High-quality ferromagnetic Josephson junctions based on aluminum electrodes, Nanomaterials **12**, 4155 (2022).

[6] H. G. Ahmad *et al.*, Hybrid ferromagnetic transmon qubit: Circuit design, feasibility, and detection protocols for magnetic fluctuations, Phys. Rev. B **105**, 214522 (2022).

[7] H. G. Ahmad *et al.*, Phase dynamics of tunnel Al-based ferromagnetic Josephson junctions, Appl. Phys. Lett. **124**, 232601 (2024).

[8] Y. Zhang, Y. Gu, P. Li, J. Hu, and K. Jiang, General theory of Josephson diodes, Phys. Rev. X **12**, 041013 (2022).

[9] J. Díez-Mérida *et al.*, Symmetry-broken Josephson junctions and superconducting diodes in magic-angle twisted bilayer graphene, Nat. Commun. **14**, 2396 (2023).

[10] J. F. Steiner, L. Melischek, M. Trahms, K. J. Franke, and F. von Oppen, Diode effects in current-biased Josephson junctions, Phys. Rev. Lett. **130**, 177002 (2023).

[11] A. Soori, Nonequilibrium Josephson diode effect in periodically driven SNS junctions, Phys. Scr. **98**, 065917 (2023).

[12] B. Lu, S. Ikegaya, P. Burset, Y. Tanaka, and N. Nagaosa, Tunable Josephson diode effect on the surface of topological insulators, Phys. Rev. Lett. **131**, 096001 (2023).

[13] H. Wu, Y. Wang, Y. Xu, P. K. Sivakumar, C. Pasco, U. Filippozzi, S. S. P. Parkin, Y. J. Zeng, T. McQueen, and M. N. Ali, The field-free Josephson diode in a van der Waals heterostructure, Nature (London) **604**, 653 (2022).

[14] J. A. Blackburn, M. Cirillo, and N. Grønbech-Jensen, A survey of classical and quantum interpretations of experiments on Josephson junctions at very low temperatures, Phys. Rep. **611**, 1 (2016).

[15] M. Suleiman, M. F. Sarott, M. Trassin, M. Badarne, and Y. Ivry, Nonvolatile voltage-tunable ferroelectric-superconducting quantum interference memory devices, Appl. Phys. Lett. **119**, 112601 (2021).

[16] E. Piatti, Ionic gating in metallic superconductors: A brief review, Nano Express **2**, 024003 (2021).

[17] G. A. Ummarino, E. Piatti, D. Daghero, R. S. Gonnelli, I. Y. Sklyadneva, E. V. Chulkov, and R. Heid, Proximity Eliashberg theory of electrostatic field-effect doping in superconducting films, Phys. Rev. B **96**, 064509 (2017).

[18] E. Piatti, D. Daghero, G. A. Ummarino, F. Laviano, J. R. Nair, R. Cristiano, A. Casaburi, C. Portesi, A. Sola, and R. S. Gonnelli, Control of bulk superconductivity in a BCS superconductor by surface charge doping via electrochemical gating, Phys. Rev. B **95**, 140501(R) (2017).

[19] A. Glezer Moshe, E. Farber, and G. Deutscher, Granular superconductors for high kinetic inductance and low loss quantum devices, Appl. Phys. Lett. **117**, 062601 (2020).

[20] M. Kim, G. H. Park, J. Lee, J. H. Lee, J. Park, H. Lee, G. H. Lee, and H. J. Lee, Strong proximity Josephson coupling in vertically stacked $NbSe_2$−graphene−$NbSe_2$ van der Waals junctions, Nano Lett. **17**, 6125 (2017).

[21] J. M. Martinis and K. Osborne, Superconducting qubits and the physics of Josephson junctions, in *Proceedings of Les Houches* (National Institute of Standards and Technology, Boulder, CO, 2004).

[22] T. Nishimatsu, U. V. Waghmare, Y. Kawazoe, and D. Vanderbilt, Fast molecular-dynamics simulation for ferroelectric thin-film capacitors using a first-principles effective Hamiltonian, Phys. Rev. B: Condens. Matter Mater. Phys. **78**, 104104 (2008).

[23] V. L. Ginzburg, Phase transitions in ferroelectrics (some historical remarks), Ferroelectrics **267**, 23 (2002).

[24] P. Chandra and P. B. Littlewood, A Landau primer for ferroelectrics, in *Physics of Ferroelectrics*, edited by K. Rabe, C. Ahn, and J.-M. Triscone, Topics in Applied Physics, Vol. 105 (Springer, Berlin, Heidelberg, 2007), pp. 69–116.

[25] M. Hoffmann, F. P. G. Fengler, M. Herzig, T. Mittmann, B. Max, U. Schroeder, R. Negrea, L. Pintilie, S. Slesazeck, and T. Mikolajick, Unveiling the double-well energy landscape in a ferroelectric layer, Nature (London) **565**, 464 (2019).

[26] I. Rahmonov, N. Chtchelkatchev, and Y. Sjukrinov, The resonance properties of superconductor/ferroelectric/superconductor heterostructure, in *7th International Workshop on Numerical Modelling of High Temperature Superconductors (HTS 2020)* (Université de Lorraine-GREEN, Nancy, France 2021).

[27] M. S. Richman, P. Rulis, and A. N. Caruso, Ferroelectric system dynamics simulated by a second-order Landau model, J. Appl. Phys. **122**, 094101 (2017).

[28] T. Yang, B. Wang, J. M. Hu, and L. Q. Chen, Domain dynamics under ultrafast electric-field pulses, Phys. Rev. Lett. **124**, 107601 (2020).

[29] G. Schön and A. D. Zaikin, Quantum coherent effects, phase transitions, and the dissipative dynamics of ultra small tunnel junctions, Phys. Rep. **198**, 237 (1990).

[30] A. O. Caldeira and A. J. Leggett, Influence of dissipation on quantum tunneling in macroscopic systems, Phys. Rev. Lett. **46**, 211 (1981).

[31] D. E. McCumber, Effect of ac impedance on dc voltage-current characteristics of superconductor weak-link junctions, J. Appl. Phys. **39**, 3113 (1968).

[32] W. C. Stewart, Current-voltage characteristics of Josephson junctions, Appl. Phys. Lett. **12**, 277 (1968).

[33] J. T. Wang, F. Tang, M. Chinkhota, R. Tashakkori, and D. Bagayoko, A theoretical model for ferroelectric polarization-controlled superconductor devices, Nucl. Instrum. Methods Phys. Res. A **410**, 304 (1998).

[34] G. A. Ummarino and D. Romanin, Theoretical explanation of electric field-induced superconductive critical temperature shifts in indium thin films, Phys. Status Solidi B: Basic Res. **257**, 1900651 (2020).

[35] F. Paolucci, G. De Simoni, E. Strambini, P. Solinas, and F. Giazotto, Ultra-efficient superconducting Dayem bridge field-effect transistor, Nano Lett. **18**, 4195 (2018).

[36] F. Paolucci, G. De Simoni, P. Solinas, E. Strambini, C. Puglia, N. Ligato, and F. Giazotto, Field-effect control of metallic superconducting systems, AVS Quantum Sci. **1**, 016501 (2019).

[37] G. De Simoni, F. Paolucci, P. Solinas, E. Strambini, and F. Giazotto, Metallic supercurrent field-effect transistor, Nat. Nanotechnol. **13**, 802 (2018).

[38] F. Paolucci, F. Vischi, G. De Simoni, C. Guarcello, P. Solinas, and F. Giazotto, Field-effect controllable metallic Josephson interferometer, Nano Lett. **19**, 6263 (2019).

[39] V. Ambegaokar and A. Baratoff, Tunneling between superconductors, Phys. Rev. Lett. **10**, 486 (1963).

[40] See Supplemental Material at http://link.aps.org/supplemental/10.1103/4746-w9cm for information on methods, additional simulation, and details.

[41] A. Grigoriev, M. M. Azad, and J. McCampbell, Ultrafast electrical measurements of polarization dynamics in ferroelectric thin-film capacitors, Rev. Sci. Instrum. **82**, 124704 (2011).

[42] D. Monroe, M. Alidoust, and I. Žutić, Tunable planar Josephson junctions driven by time-dependent spin-orbit coupling, Phys. Rev. Appl. **18**, L031001 (2022).

[43] F. Wen, J. Shabani, and E. Tutuc, Josephson junction field-effect transistors for Boolean logic cryogenic applications, IEEE Trans. Electron Devices **66**, 5367 (2019).

[44] I. Holzman and Y. Ivry, On-chip integrable planar NbN nanoSQUID with broad temperature and magnetic-field operation range, AIP Adv. **9**, 105028 (2019).

[45] P. Winkel, K. Borisov, L. Grünhaupt, D. Rieger, M. Spiecker, F. Valenti, A. V. Ustinov, W. Wernsdorfer, and I. M. Pop, Implementation of a transmon qubit using superconducting granular aluminum, Phys. Rev. X **10**, 031032 (2020).

[46] R. Li, D. Xu, C. Du, Q. Ma, F. Zhang, X. Liang, D. Wang, Z. Shi, W. Liu, and D. Zhou, Giant dielectric tunability in ferroelectric ceramics with ultralow loss by ion substitution design, Nat. Commun. **15**, 3754 (2024).

[47] Y. Gao, A. Weston, V. Enaldiev, X. Li, W. Wang, J. E. Nunn, I. Soltero, E. G. Castanon, A. Carl, and H. De Latour, Tunnel junctions based on interfacial two dimensional ferroelectrics, Nat. Commun. **15**, 4449 (2024).

[48] I. M. Pop, I. Protopopov, F. Lecocq, Z. Peng, B. Pannetier, O. Buisson, and W. Guichard, Measurement of the effect of quantum phase slips in a Josephson junction chain, Nat. Phys. **6**, 589 (2010).

[49] T. Liang, G. Zhang, W. Wu, Y. Wang, L. Zhang, H. Jin, X. Zhang, L. Ying, and B. Gao, Fabrication and characterization of molybdenum thin-film resistor for superconducting quantum devices, IEEE Trans. Appl. Supercond. **30**, 7500304 (2020).